Proceedings of The National Conference
On Undergraduate Research (NCUR) 2019
Kennesaw State University
Kennesaw, Georgia
April 11-13, 2019

Comparative Study of Carbonaceous Meteorites using micro-Raman Spectroscopy and SEM/EDS

Rohil Kayastha, Raka Paul, and Aaron Stokke
Physics
Minnesota State University - Mankato
Mankato, Minnesota 56001 USA

Faculty Advisor: Dr. Analía Dall'Asén

Abstract

The formation of the planets in our solar system is not fully understood. Carbonaceous chondritic meteorites, considered the most primitive surviving materials from the early Solar System, can contribute to the understanding of how planets formed from dust through the study of their composition. These relics are mainly composed of chondrules (micro/millimeter-sized inclusions) surrounded by a matrix of microparticles. The mineralogical composition of the chondrules and surrounding matrix of these meteorites can be characterized at the microscale using micro-Raman spectroscopy, while the topography and elemental composition of these relics can be studied at the micro/nanoscale using SEM/EDS (Scanning Electron Microscopy/Energy Dispersive X-ray Spectroscopy). In this work, we present a comparative study of the mineralogical and elemental composition of the chondrules and surrounding matrix of carbonaceous chondritic meteorites using the aforementioned techniques. We examine how these properties vary in different regions of the chondrules and matrix. In general, Raman spectroscopy results show graphite, pyroxene, and olivine, both within and outside the chondrules. Well-defined chondrules, rims, and matrix are observed from the SEM images. The results obtained with EDS show that iron is most abundant in the matrix, while the chondrules are enhanced in magnesium. Silicon, aluminum, sodium, calcium, oxygen, and carbon are also found in both, chondrules and matrix. Iron and sulfur rims are observed around the chondrules. These findings contribute detailed information about the composition of these chondritic meteorites, helping to understand the origin of the found structures and to unravel the mysteries surrounding the formation of these relics.

Keywords: Carbonaceous Meteorites, Raman Spectroscopy, Scanning Electron Microscopy

1. Introduction

The formation of the solar system has attracted many scientists from different disciplines for a long time. Even though numerous theoretical and experimental studies have been conducted to learn about its origin, the whole process of planet formation is not fully understood. One approach to analyze the origin of the Solar System is to study carbonaceous chondritic meteorites.[1] These chondrites are some of the most primitive materials of our Solar System and are accessible on Earth. They are composed of inclusions, such as chondrules, crystals, calcium-aluminum-rich inclusions (CAIs), and amoeboid-olivine aggregates (AOAs), which are embedded in a matrix that keeps the chondrite together. Chondrules are formed due to flash melting at high temperature creating a molten droplet making their shape spherical.[2, 3] CAIs and AOAs are refractory inclusions that contain elements or minerals that were unaffected by heat and wear. AOAs are irregularly shaped and have a high amount of forsterite (Mg-rich olivine), while CAIs contain minerals rich in Ca and Al.[3]

By studying experimentally several properties of the inclusions and matrix of carbonaceous chondritic meteorites (e.g. topography, mineralogical and elemental composition, etc.), important information about planet formation and the secondary processes that affected their parent bodies (such as asteroids and comets) can be found. For this, several

techniques, such as Raman spectroscopy, scanning electron microscopy (SEM), energy dispersive X-ray spectroscopy (EDS), and optical microscopy can be used.[1] In this work, these techniques were employed to characterize two different carbonaceous chondrites: Nogoyá and Allende. Nogoyá belongs to the CM2 group, where "C" stands for carbonaceous, "M" stands for "Mighei" (Ukraine) corresponding to the location where the most prominent meteorite with similar composition originated, and "2" represents its petrologic type corresponding to the least aqueous alteration in the parent body. Allende belongs to the CV3 group, where "C" stands for carbonaceous, "V" stands for "Vigarano" (Italy) and the petrologic type "3" refers to the least thermally altered chondrites in its parent body.[4, 5] To the best of the authors' knowledge, Nogoyá has been barely studied with the aforementioned techniques[2, 6] thus this study can provide more information about its composition, and it is compared with Allende which is a better-known carbonaceous chondritic sample.[2, 7]

2. Experimental Methods

2.1. Samples

Two different samples of carbonaceous chondritic meteorites were used for this study: Nogoyá and Allende. Nogoyá is a CM2 type carbonaceous chondritic meteorite which was an observed fall in Nogoyá (Entre Ríos, Argentina) in 1879.[8] Figure 1a shows a very small fragment of Nogoyá used for this project which weighs 0.0578 g and has a size of ~8.9 mm x 3.5 mm. Allende is a CV3 type carbonaceous chondritic meteorite and was an observed fall in the village of Pueblito de Allende (Chihuahua, Mexico) in 1969.[9] Figure 1b shows the Allende fragment used for this work which weighs 5.1916 g and has dimensions of ~22.3 mm x 20.6 mm. No sample preparation was required for the experimental techniques employed in this project. Figure 1 also shows the regions selected for each sample, marked in yellow circles, to be analyzed using different nondestructive characterization techniques.

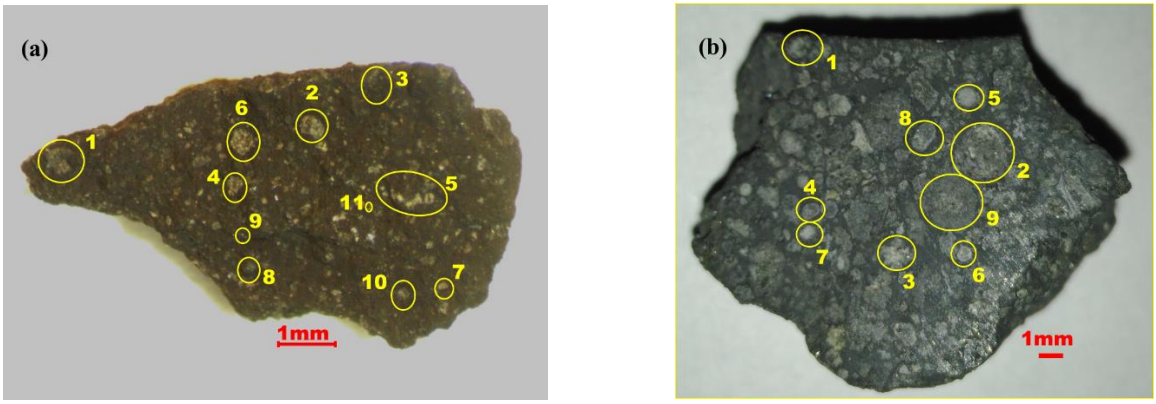

Figure 1. Photographs of carbonaceous chondrite fragments: (a) Nogoyá; and (b) Allende. The yellow circles mark the selected regions including inclusions and surrounding matrix.

2.2. Raman Spectroscopy

In order to study the mineralogical properties of the sample, a custom-built fiber-coupled micro-Raman system with a backscattering configuration was used. The Raman system had a 10X objective with a numerical aperture of 0.25 and 300 mm focal length spectrometer (Andor SR-303i-A). Both low- and high-resolution measurements were carried out using gratings of 600 lines mm^{-1} and 1200 lines mm^{-1}, respectively. A 532-nm line of linearly polarized semiconductor laser (Coherent Sapphire SF 532 nm) was employed for the excitation of the sample. A power of ~5 mW and a focal spot of diameter ~3 μm were used on the meteorite fragments, producing a low power density on the samples (~0.707 $\mu W \mu m^{-2}$) to avoid laser-induced alterations. A thermo-cooled charge-coupled device (CCD) camera (Andor iDus DU401A-BVF) was used to detect the Raman-scattered light from the same objective. Individual spectra were taken from the selected spots of the examined regions on the meteorite, using an integration time of 1 second and 1 to 100 accumulations depending on the signal-to-noise ratio.[1] In order to analyze the mineralogical composition of the

samples, a commercial software package (OriginPro 2018) was used to fit Gaussian and Lorentzian functions to the spectrum peaks to determine their peak position, full width at half maximum, and intensity.

2.3. SEM/EDS

In order to study the topography and elemental composition of the samples, a combined system containing an SEM (JEOL JSM-6510LV) and an EDS detector (Thermo Scientific UltraDry) was used. The sample was treated under high-vacuum conditions with a beam potential of 15-20 kV. The samples were analyzed using magnifications from 30X to 3000X. Two different types of SEM detection, secondary electron (SE) and backscatter electron (BSE), were used. The SE detection provides the topographical composition of the surface of the sample up to ~9 nm,[10] while the BSE detection gives sample information from deeper areas than SE and produces composition contrast images where brighter regions correspond to elements with higher atomic numbers. SEM images and EDS spectra were taken from the selected regions including those where Raman spectroscopy measurements were performed. From the EDS measurements, maps of elements of the samples were acquired.

3. Results

3.1. Raman spectroscopy

Figures 2 and 3 show representative low- and high-resolution Raman spectra obtained from selected spots of Nogoyá and Allende, respectively.

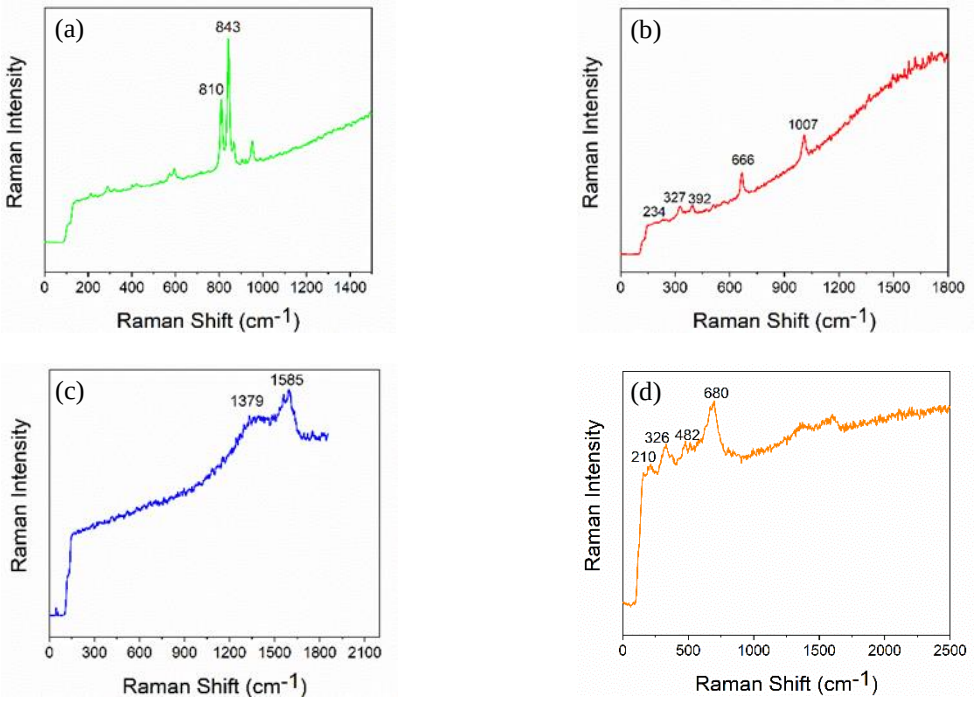

Figure 2. Representative low- and high-resolution Raman spectra of main materials found in Nogoyá. Only peaks corresponding to the respective mineral are labeled. Peaks were fitted using Gaussian and Lorentzian functions: (a) olivine with a high content of fayalite; (b) pyroxene with a high content of diopside; (c) amorphous carbon; and (d) unidentified mineral.

Figure 2 shows the Raman spectra of the three main minerals found in Nogoyá: olivine, pyroxene, and amorphous carbon. The highlighted peaks with numbers next to them are the representative peaks of each mineral, while other peaks that are not labeled are part of other minerals. In Figure 2a, an olivine crystal with a doublet at ~810/843 cm^{-1}

was obtained from the inclusion of region 7 (Fig. 1a). These characteristics are the result of the coupled symmetric and antisymmetric stretching modes of nonbridging Si-O_{nb} bonds in the SiO4 tetrahedra.[1, 11] The percentage composition of fayalite (Fe_2SiO_4) and forsterite (Mg_2SiO_4) can be determined by looking at the peak positions of the olivine spectra doublet, thus the olivine crystals found have a high fayalite content.[11] Figure 2b shows a high-calcium pyroxene spectrum obtained from the inclusion in region 10 (Fig. 1a) with peaks at ~1007, 666, 392, 327, and 234 cm^{-1} corresponding to high content of diopside ($Mg_2CaSi_2O_6$).[1] The first two peaks are due to symmetrical stretching of the nonbridging Si-O_{nb} and bridging Si-O_b-Si bonds, respectively.[1, 12, 13] Figure 2c shows the characteristic bands of amorphous carbon which was obtained from the matrix (region 8 in Fig. 1a): the G-band at ~1585 cm^{-1} due to the stretching of C-C bonds, with a broad shoulder corresponding to the D-band at ~1379 cm^{-1} due to the defects found in the crystal structure of carbon.[1] An unidentified spectrum of a mineral was found with the main peaks at ~680, 482, 326, and 210 cm^{-1} (Fig. 2d). This unknown mineral was found in the matrix of regions 5 and 8 (Fig. 1a).

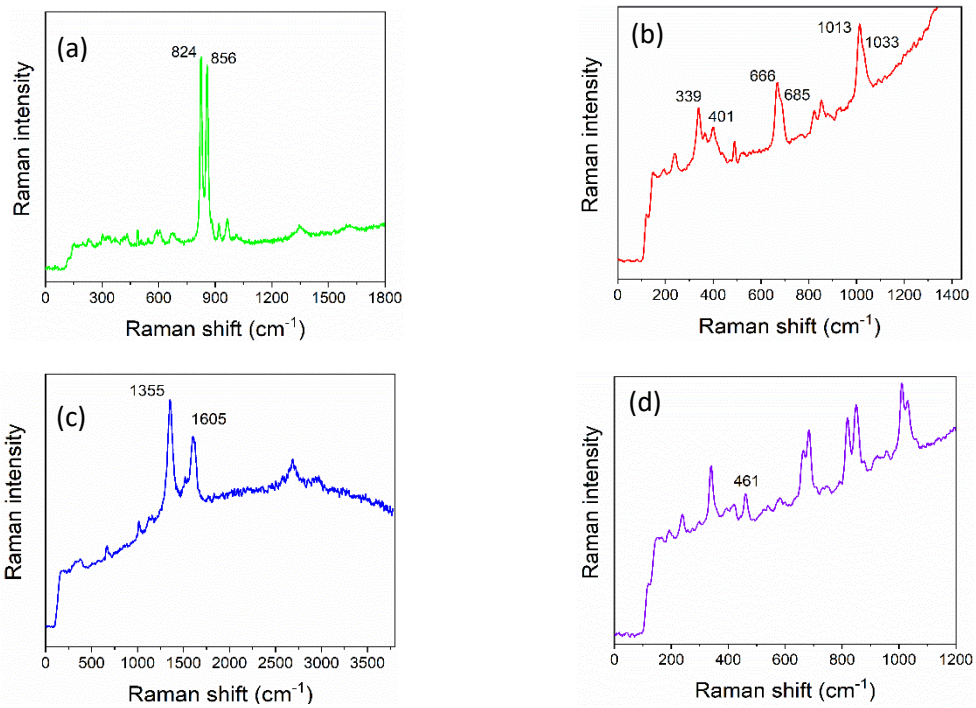

Figure 3. Representative low- and high-resolution Raman spectra of main materials found in Allende. Only peaks corresponding to the respective mineral are labeled. Peaks were fitted using Gaussian and Lorentzian functions: (a) olivine with a high content of forsterite; (b) pyroxene with a high content of enstatite; (c) graphitic carbon; and (d) quartz.

Figure 3 shows representative Raman spectra of the main four minerals found in Allende[7]: olivine, pyroxene, graphitic carbon, and quartz. An olivine doublet at ~824/856 cm^{-1}, indicating a high content of forsterite[11] obtained from inclusion 7 (Fig. 1b), is shown in Figure 3a. High content of enstatite ($MgSiO_3$), low-calcium pyroxene, was found in region 4 (Fig. 1b), which main peaks are at ~1033/1013, 685/666, 401, and 339 cm^{-1} (Fig. 3b).[1] The Raman spectrum of graphitic-like carbon shows narrower peaks for D- and G-bands than those ones corresponding to amorphous carbon. Figure 3c shows the graphitic-like spectrum obtained from the matrix with D-band at ~1355 cm^{-1} and G-band at ~1605 cm^{-1}. Quartz (SiO_2) was found from region 5 (Fig. 1b) with a main peak at ~461 cm^{-1} (Fig. 3d).[14]

3.2. SEM/EDS

Figures 4 to 8 show SE- and BSE-SEM images and EDS maps of Nogoyá and Allende with distinct topographical and elemental compositional features that have been observed.

Figure 4 shows the SE-SEM image of the whole region 8 (Fig. 1a) in Nogoyá with a crystal and surrounding matrix, and the BSE-SEM image and EDS map of a distinct structure found in region 8 spot 1 (marked with a red circle in the

SE figure). From the EDS maps and Raman results, the SE image of region 8 was identified as an olivine crystal. The magnified BSE image of spot 1 reveals a ~20-µm structure which is composed of only C, as the EDS maps of C, Mg, and Fe clearly exhibit in Figure 4. Figure 5 shows the BSE-SEM image of the whole region 9 (Fig. 1a) in Nogoyá with the EDS maps of Mg, S, Si, Ca and Fe. The BSE-SEM image reveals the topography of an olivine crystal with high content of forsterite (Mg-rich olivine) determined by the Raman results and EDS maps. The complementarity between Fe and Mg can be observed with an absence of Fe and abundance of Mg in the inclusion, and vice versa in the matrix. In some regions, this complementarity with Fe also includes Si in the same spots as Mg. A correlation between S and Ca is also observed throughout the region. Figure 6 shows the BSE-SEM image of the whole region 6 (Fig. 1a) in Nogoyá with a magnified SE-SEM image and EDS maps of spot 1. Similar to Figure 5, the Fe/Mg complementarity is observed. In addition, both patches of Al and a correlation between S and Ni can be distinguished.

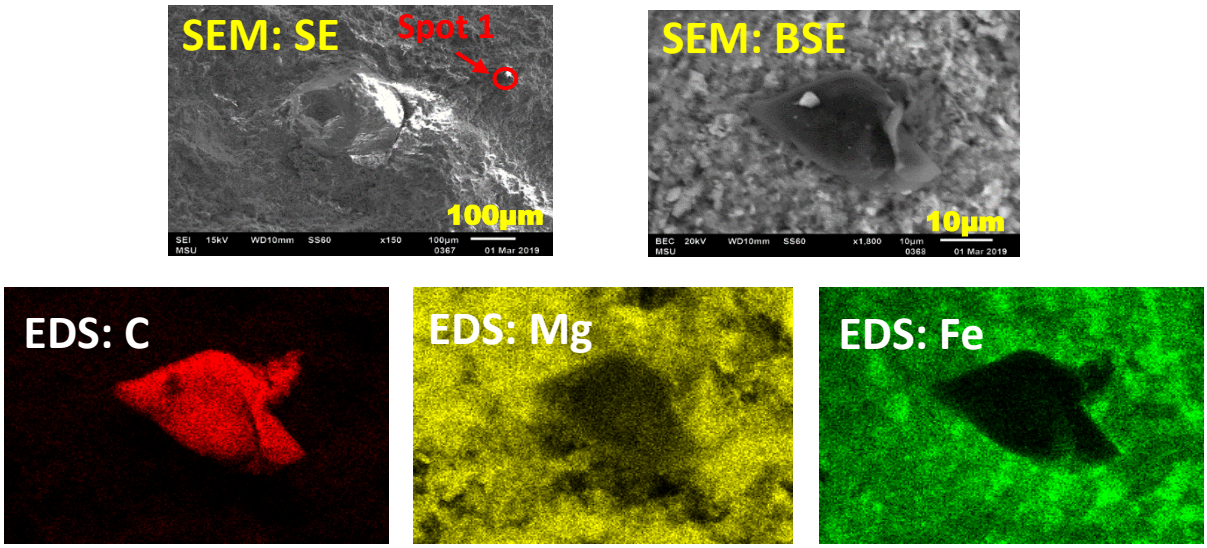

Figure 4. SE and BSE-SEM images and EDS maps of Nogoyá from region 8 (Fig. 1a) at 140X magnification (SE-SEM) and region 8 spot 1 at 1800X magnification (BSE-SEM/EDS). SEM/EDS images show the topography and composition of the inclusion and adjacent matrix. EDS maps show a patch of C.

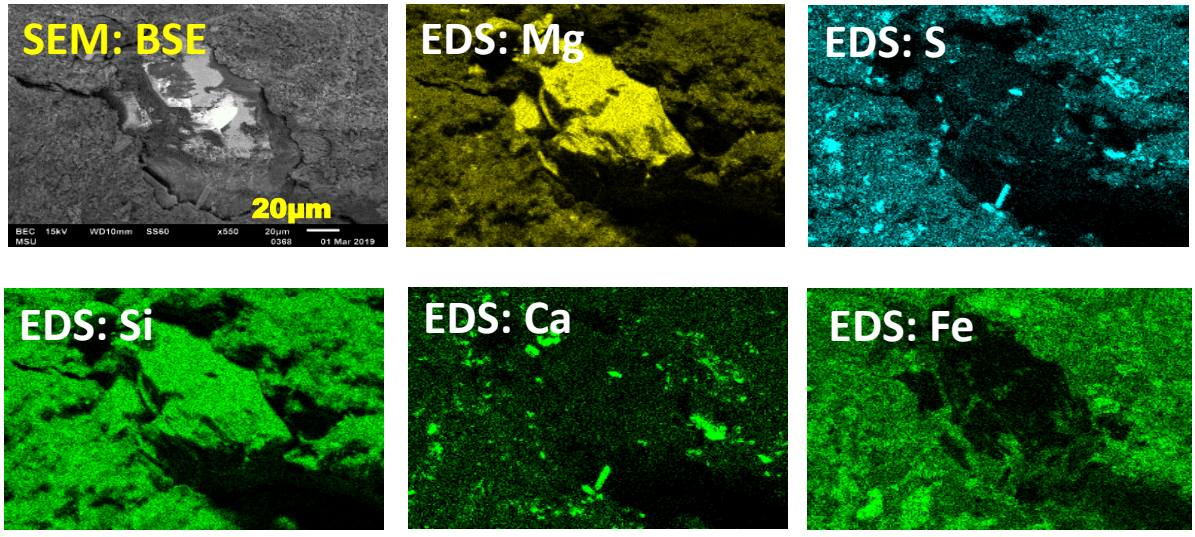

Figure 5. SE and BSE-SEM images and EDS maps of Nogoyá from region 9 (Fig. 1a) at 550X magnification (BSE-SEM/EDS). SEM/EDS images show the topography and composition of the inclusion and adjacent matrix. EDS maps show correlations for Mg-Si-Fe and S-Ca.

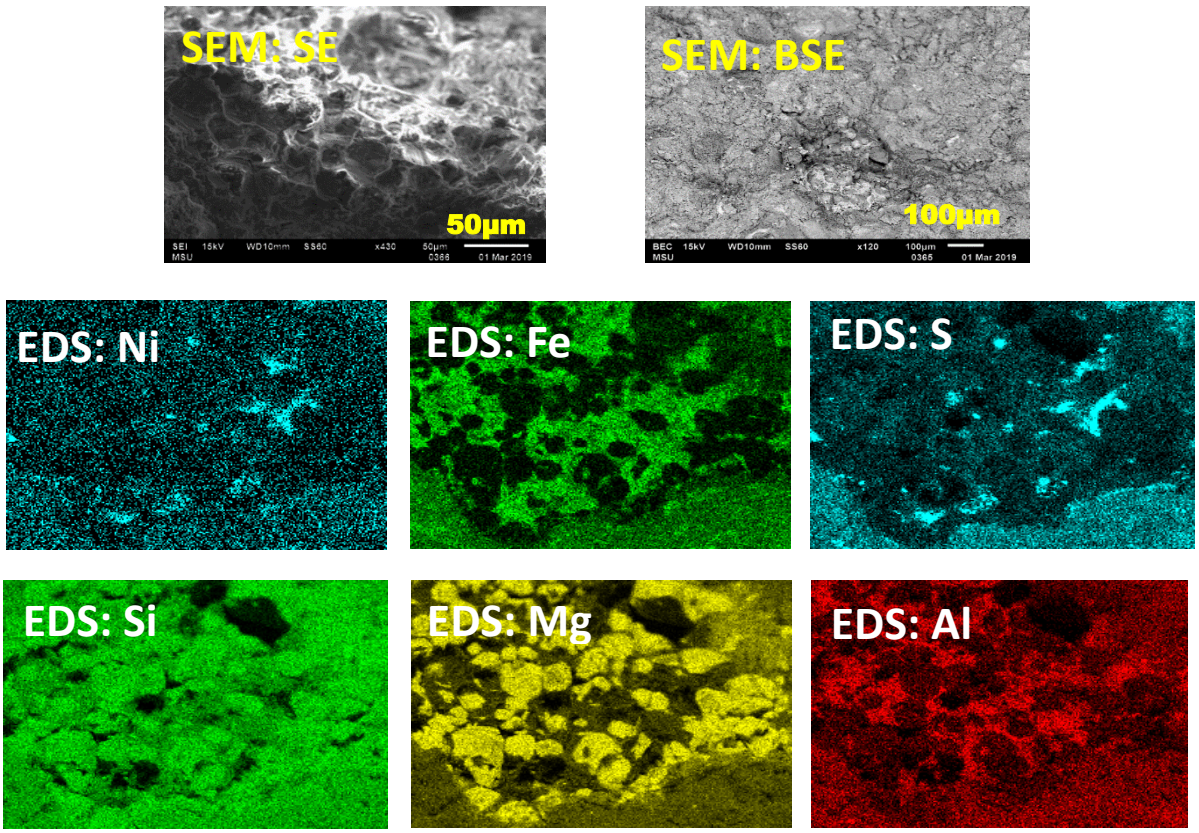

Figure 6. SE and BSE-SM images, and EDS maps of Nogoyá from region 6 (Fig. 1a) at 120X magnification (BSE-SEM) and region 6 at 430X magnification (SE-SEM/EDS). SEM/EDS images show the topography and composition of the inclusion and adjacent matrix. EDS maps show correlations for Mg-Si-Fe, and S-Ni, and patches of Al.

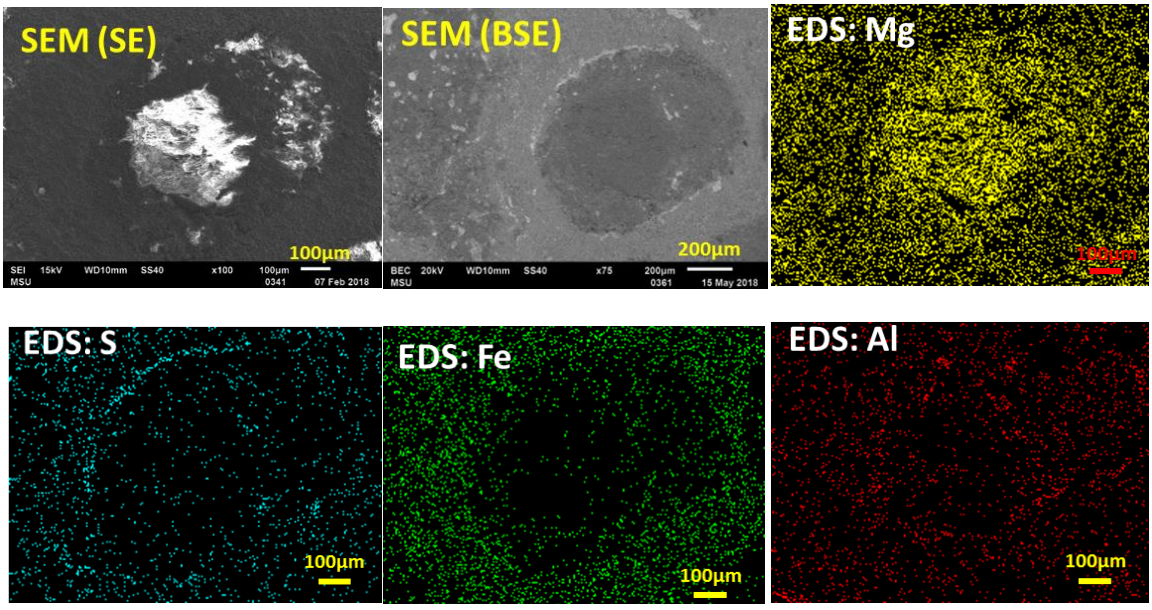

Figure 7. SE and BSE-SEM images and EDS maps of Allende's region 4 (Fig. 1b) at 100X magnification (SE-SEM/EDS) and 75X magnification (BSE-SEM). SEM/EDS images show the topography and composition of the inclusion and adjacent matrix. EDS maps show correlations between Mg-Fe, patches of Al, and an S rim.[7]

Figure 7 shows SE- and BSE-SEM images and EDS elemental maps of region 4 (Fig. 1b) in Allende. In the BSE-SEM image, a clear contrast between the inclusion and the matrix is observed. The EDS maps show a correlation between Fe and Mg, and an S rim around the inclusion. A higher concentration of Fe and S can be observed in the matrix whereas Mg is dominant in the inclusion. In addition, patches of Al can be seen throughout the region. Figure 8a shows a SE-SEM image of an inclusion found in region 3 (Fig. 1b) in Allende. The region marked with a green circle is magnified in Figure 8b showing an EDS map of C over the SE-SEM image. Several patches of C can be observed. In particular, the region marked with a yellow circle is magnified in the SE-SEM image in Figure 8c showing a distinct flat layer-like structure corresponding to a zone with high content of C, as shown in the EDS map of C in Figure 8d.[7]

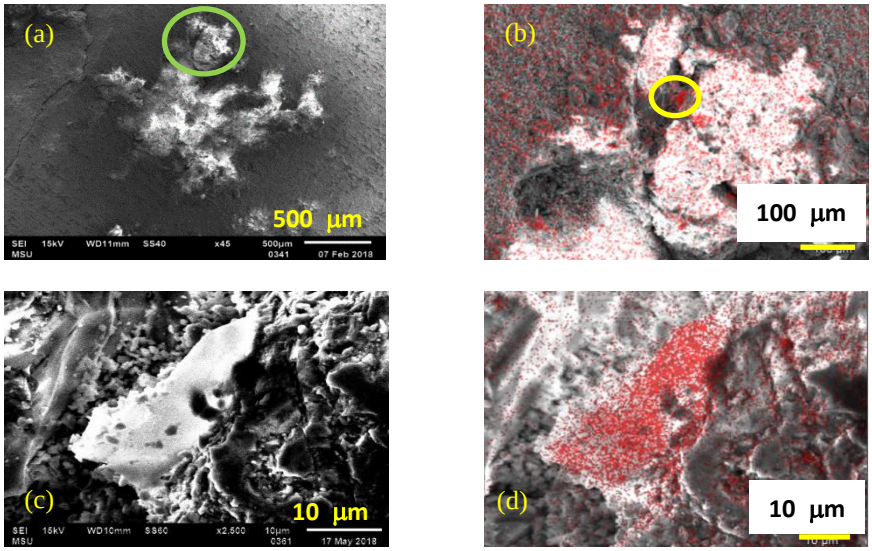

Figure 8. (a) SE-SEM image of region 3 (Fig. 1b) in Allende (45X magnification); (b) SEM close up with EDS C map (250X magnification) of region marked in (a) with a green circle; (c) SEM close up of a C-rich structure (2500X magnification) identified in (b) with a yellow circle; (d) EDS C-rich map on SEM image shown in (c).[7]

4. Discussion

The main purpose of this paper is to study the mineralogical and elemental composition of the barely analyzed carbonaceous chondritic meteorite Nogoyá, and compare its properties with the better-known carbonaceous chondritic fragment Allende, using micro-Raman spectroscopy and SEM/EDS in the same experimental conditions.

By visual inspection using a white light illumination optical microscope, it was possible to observe that the Nogoyá sample presented less inclusions per unit area than the Allende sample, which is characteristic of the CM and CV meteorites, respectively.[15] From all the employed techniques, the inclusions studied for both samples showed typical characteristics of chondrules with a circular shape and well-defined boundaries (e.g. inclusions in regions 2, 6 and 10 for Nogoyá, and in regions 1, 4-9 for Allende) and potential AOA inclusions with irregular shapes (e.g. inclusion in region 5 for Nogoyá, and in region 3 for Allende). In addition, Nogoyá presented olivine crystals, both fayalite and forsterite (e.g. inclusions in region 7-9), while Allende exhibited a potential CAI due its circular shape and composition of Ca and Al (e.g. inclusion in region 2).[3, 7]

Both samples showed similar general distinct mineralogical and elemental compositions. The chondrules presented a higher relative composition of Mg and Si, while the composition in Fe was low. They were also rich in Al, Na and Ca. Olivine (fayalite and forsterite) and pyroxene (diopside and enstatite) were the dominant minerals in the chondrules. The matrix presented a relative high composition of Fe, and it was also rich in S and Ni around the chondrules. Complementarity between Fe and Mg was observed in both meteorites. Other elements such as O, C, Ni, Na, Ca and Cr were also found in both inclusions and matrix.

On the other hand, the studied samples showed different noticeable features. First, mostly S rims were found in Allende. In addition, even though the EDS results revealed carbon patches in both samples, they were identified by Raman spectroscopy as mostly amorphous carbon in Nogoyá, whereas graphitic carbon was seen in Allende. Both

minerals were dominate materials in their respective samples. Furthermore, numerous olivine crystals were observed in Nogoyá, while the inclusions studied in Allende did not correspond to this kind of structure. Finally, some unidentified minerals (e.g. shown in Fig. 2d) were only found in Nogoyá, and quartz was only observed in Allende.

These results provided detailed identification of the composition of the Nogoyá sample and its comparison with the Allende fragment, contributing to more information about this carbonaceous chondritic meteorite.[2, 6]

Future work will focus on identifying the unknown minerals by comparing the obtained spectra and EDS maps with scientific literature and available Raman spectra databases (e.g. RRUFF[16]). In addition, the Raman spectra peaks of the carbon material found in the meteoritic fragments will be analyzed to study their relative degree of graphitization/amorphization, and thus to determine the peak metamorphic temperature (PMT) of their parent bodies, which will provide information about secondary processes that affected them (e.g. thermal metamorphism).[7, 17-19] Furthermore, these findings will be compared with those obtained from other meteoritic samples (e.g. Bali[7], Moss[17]), to understand the origin of the found structures. For example, the chondrule-matrix chemical complementarity observed in carbonaceous chondrites (e.g. between Fe and Mg) suggests that the formation of chondrules and matrix could have occurred by similar processes from a single chondritic nebular reservoir;[7,20, 21] and the S rims could have formed due to chondrules initially free-floating in solar nebular where rim materials were originally present.[22, 23] Therefore, these findings will help to uncover the mysteries regarding the formation of these primitive bodies.

5. Acknowledgments

The authors would like to express their sincere gratitude to Dr. Michael Bentley who generously allowed them to access the SEM/EDS equipment, Mr. Mike Peters for his technical support, and Dr. Russell Palma for providing various meteoritic samples (Dept. of Biological Sciences, and Dept. of Physics and Astronomy, Minnesota State University-Mankato, respectively). This research was funded in part by Minnesota State University-Mankato Faculty Research and Undergraduate Research Center grants.

6. References

1. Dall'Asén, A. G., Dimas, S. I., Tyler, S., Johnston, J. F., Anderton, T. R., Ivans, I. I., Gerton J. M., Bromley, B. C., and Kenyon, S. J. (2017). Mapping the composition of chondritic meteorite Northwest Africa 3118 with micro-Raman spectroscopy. *Spectroscopy Letters*, 50(8), 417–425; and references therein. https://doi.org/10.1080/00387010.2017.1346689

2. Russell, S., Connolly Jr., H., and Krot, A. (Eds.). (2018). *Chondrules: Records of Protoplanetary Disk Processes* (Cambridge Planetary Science). Cambridge, UK: Cambridge University Press. https://doi.org/10.1017/9781108284073

3. McSween, H. Y., and Huss, G. R. (2010). *Cosmochemistry: probing the origin and chemical evolution of the solar system*. Cambridge, UK: Cambridge University Press.

4. McSween, H. Y. (1999). *Meteorites and their parent planets* (2nd ed.). Cambridge, UK; New York, NY: Cambridge University Press.

5. Weisberg, M. K., McCoy, T. J., and Krot, A. N. (2006). Systematics and Evaluation of Meteorite Classification. In D. S. Lauretta & H. Y. McSween (Eds.), *Meteorites and the Early Solar System II* (pp. 19-52). Tucson, AZ: The University of Arizona Press.

6. Chan, Q. H.S., Zolensky, M. E., Bodnar, R. J., Farley, C., and Cheung, J. C. H. (2017). Investigation of organo-carbonate associations in carbonaceous chondrites by Raman spectroscopy. *Geochimica et Cosmochimica Acta*, 201, 392-409. https://doi.org/10.1016/j.gca.2016.10.048

7. Paul, R. (2018). Comparative study of CV3 carbonaceous chondrites Allende and Bali using micro-Raman spectroscopy and SEM/EDS. *All Theses, Dissertations, and Other Capstone Projects*. 837; and references therein. https://cornerstone.lib.mnsu.edu/etds/837

8. Meteoritical Bulletin Database: Entry for Nogoya. (n.d.). Retrieved Winter, 2018, from https://www.lpi.usra.edu/meteor/metbull.php?sea=Nogoya&sfor=names&ants=&nwas=&falls=&valids=&stype=contains&lrec=50&map=ge&browse=&country=All&srt=name&categ=All&mblist=All&rect=&phot=&strewn=&snew=0&pnt=Normal%20table&code=16989

9. Meteoritical Bulletin Database: Entry for Allende. (n.d.). Retrieved Summer, 2018, from https://www.lpi.usra.edu/meteor/metbull.php?sea=Allende&sfor=names&ants=&nwas=&falls=&valids=&stype=contains&lrec=50&map=ge&browse=&country=All&srt=name&categ=All&mblist=All&rect=&phot=&strewn=&snew=0&pnt=Normal%20table&code=2278

10. Goldstein, J., Newbury, D. E., Michael, J. R., Ritchie, N. W., Scott, J. H., and Joy, D. C. (2018). *Scanning electron microscopy and x-ray microanalysis* (4th edition). New York, NY: Springer. https://doi.org/10.1007/978-1-4939-6676-9

11. Kuebler, K. E., Jolliff, B. L., Wang, A., and Haskin, L. A. (2006). Extracting olivine (Fo–Fa) compositions from Raman spectral peak positions. *Geochimica et Cosmochimica Acta*, 70(24), 6201–6222. https://doi.org/10.1016/j.gca.2006.07.035

12. Mernagh, T. P., and Hoatson, D. M. (1997), Raman spectroscopic study of pyroxene structures from the Munni Munni layered intrusion, Western Australia. *Journal of Raman Spectroscopy*, 28, 647-658. doi:10.1002/(SICI)1097-4555(199709)28:9<647::AID-JRS155>3.0.CO;2-H

13. Sharma, S. K., Lucey, P. G., Ghosh, M., Hubble, H. W., and Horton, K. A. (2003). Stand-off Raman spectroscopic detection of minerals on planetary surfaces. *Spectrochimica Acta Part A: Molecular and Biomolecular Spectroscopy*, 59(10), 2391–2407. https://doi.org/10.1016/S1386-1425(03)00080-5

14. Sharma, S. K, Mammone, J. F., and Nicol, M. F. (1981). Raman investigation of ring configurations in vitreous silica. *Nature*, 292(5819), 140-141. https://doi.org/10.1038/292140a0

15. Buseck, P. R., and Hua, X. (1993). Matrices of carbonaceous chondrite meteorites. *Annual Review of Earth and Planetary Science*, 21, 255–305.

16. RRUFF Database: Raman, X-ray, Infrared, and Chemistry. (n.d.). Retrieved Winter, 2018, from http://rruff.info/

17. Stokke, A. (2018). Compositional and Topographical Characterization of Carbonaceous Chondritic Meteorites Moss and Murray Using micro-Raman Spectroscopy and SEM/EDS. *All Theses, Dissertations, and Other Capstone Projects*. 819; and references therein. https://cornerstone.lib.mnsu.edu/etds/819

18. Busemann H., Alexander M. O., and Nittler L. R. 2007. Characterization of insoluble organic matter in primitive meteorites by microRaman spectroscopy. *Meteoritics & Planetary Science*, 42(7-8), 1387–1416. https://doi.org/10.1111/j.1945-5100.2007.tb00581.x

19. Homma, Y., Kouketsu, Y., Kagi, H., Mikouchi, T., and Yabuta, H. (2015). Raman spectroscopic thermometry of carbonaceous material in chondrites: four–band fitting analysis and expansion of lower temperature limit. *Journal of Mineralogical and Petrological Sciences*, 110(6), 276–282. https://doi.org/10.2465/jmps.150713a

20. Hezel, D. C., and Palme, H. (2010). The chemical relationship between chondrules and matrix and the chondrule matrix complementarity. *Earth and Planetary Science Letters*, 294(1–2), 85–93. https://doi.org/10.1016/j.epsl.2010.03.008

21. Palme, H., Hezel, D. C., and Ebel, D. S. (2015). The origin of chondrules: Constraints from matrix composition and matrix-chondrule complementarity. *Earth and Planetary Science Letters*, 411, 11–19. https://doi.org/10.1016/j.epsl.2014.11.033

22. Sears, D. (2004). *The Origin of Chondrules and Chondrites* (Cambridge Planetary Science). Cambridge, UK: Cambridge University Press. https://doi.org/10.1017/CBO9780511536137

23. Hewins, R. H. (1991). Retention of sodium during chondrule melting. *Geochimica et Cosmochimica Acta*, 55(4), 935–942. https://doi.org/10.1016/0016-7037(91)90152-U